2014
International Symposium on Power Electronics,
Electrical Drives, Automation and Motion

Hybrid Active-Flux and Arbitrary Injection Position Sensorless Control of Reluctance Synchronous Machines

Francois J.W. Barnard, Wikus T. Villet and Maarten J. Kamper (SMIEEE)
Department of Electrical & Electronic Engineering
University of Stellenbosch
Stellenbosch, South Africa

***Abstract*—A new hybrid position sensorless control method for reluctance synchronous machine drives is presented in this paper. The active-flux and arbitrary injection position estimation techniques are combined for the first time in this hybrid controller. The controller switches between estimation techniques depending on speed and load. A hysteresis region is implemented with phase-locked loop synchronisation for dynamic and stable changeover between estimators. Implementation of the active-flux method at high loads allows for extended sensorless torque capabilities at high speed.**

***Index Terms*—Position Sensorless Control, Hybrid Controller, Reluctance Synchronous Machine Drives**

I. Introduction

In recent years the search for high efficiency permanent magnet-less motor drives has led to considerable attention being paid to the reluctance synchronous machine (RSM) [1].

RSMs have notable application possibilities in the fields of multi-gear electrical drives [2], high speed geared wind generator systems [3] and especially, industrial drives [4]. Efficient control of the RSM (using field-oriented control [5]) requires rotor position information which is conventionally supplied by a hardware sensor. These sensors are typically unreliable and expensive compared to the rest of a lower power drive system, increasing overall cost. This motivates the use of rotor position estimation.

Estimation techniques are mainly divided into fundamental model/back EMF schemes, and saliency-based signal injection methods. Fundamental model techniques [6]-[8] make use of flux/inductance estimation by means of a machine model or back EMF measurement. These methods perform reliably at higher speeds, but fail at low speeds. Saliency based methods [9]-[13] exploit the angular-separated difference in rotor inductance for position estimation by means of signal excitation. These methods are able to track the rotor angle even at standstill, but have limited torque capabilities because of the injected signal voltage and saliency shift at higher speed. Considering the capabilities of the various estimation methods it is evident that with their combination, as in [14]-[17], position information with full torque capabilities in the entire speed range is attainable.

A hybrid position sensorless control (PSC) scheme based on the active-flux (AF) and arbitrary injection (AI) based methods presented in [15] and [11] respectively is presented in this paper. It was found that the typical hybrid controller approach of using the different estimation schemes in certain speed ranges was not viable in this case, because of the AF and AI specific current requirements for producing active flux (d-axis current) and having a large enough saliency (q-axis current). Constant current angle control is implemented for maximum torque per ampere (MTPA) (close to maximum efficiency), implying variable d-axis current. The AI method is parameter insensitive and requires a smaller injection voltage than other saliency-based methods, allowing extended torque capabilities. Consequently, a novel speed and load dependent scheme was derived which implements the AF method in the higher speed high load range and AI elsewhere. The combination of these two methods also allows the possible application of this hybrid controller to any synchronous machine.

It should be noted that an interior permanent magnet synchronous machine (which exhibits saliency without the presence of current) is used in [8] - allowing constant d-axis current for active flux. The axially laminated anisotropic RSM in [15] also has inherent saliency without the presence of q-axis current (as opposed to the normal transverse laminated rotor RSM with punched rotor flux barriers used herein). Lastly, the fundamental saliency technique used in [17] (for higher speeds) requires the presence of q-axis current - coinciding with the high-frequency injection technique used.

II. Reluctance Synchronous Machine Model

A. Mathematical Model

The motor voltage equation in stator and rotor reference frames are equal to respectively

$$\boldsymbol{v}_s^s = R_s \boldsymbol{i}_s^s + \frac{d}{dt}\boldsymbol{\psi}_s^s \tag{1}$$

and

$$\boldsymbol{v}_s^r = R_s \boldsymbol{i}_s^r + \frac{d}{dt}\boldsymbol{\psi}_s^r + j\omega_e \boldsymbol{\psi}_s^r \tag{2}$$

where $\boldsymbol{v}_s^s = v_\alpha + jv_\beta$, $\boldsymbol{v}_s^r = v_d + jv_q$ and $\boldsymbol{v}_s^s = \mathbf{T}\boldsymbol{v}_s^r$ where

$$\mathbf{T} = \begin{bmatrix} \cos\theta_e & -\sin\theta_e \\ \sin\theta_e & \cos\theta_e \end{bmatrix} \tag{3}$$

$$\mathbf{T}^{-1} = \mathbf{T}^T. \tag{4}$$

v, i, ψ and ω_e are voltage, current, flux linkage and angular electrical rotor speed respectively. R_s is the stator resistance and θ_e is the electrical rotor angle.

Vector transformation from the rotor reference frame (d-q) to the stator reference frame (α-β) are done using $\mathbf{T}$, whereas transformation from the stator reference frame to the rotor reference frame are done using $\mathbf{T}^{-1}$.

Assuming a linear dependence of flux linkage on stator current in the rotor reference frame results in the following [18]:

$$\boldsymbol{\psi}_s^r = \boldsymbol{L}_s^r \boldsymbol{i}_s^r \tag{5}$$

$$\boldsymbol{\psi}_s^s = \mathbf{T}\boldsymbol{L}_s^r \mathbf{T}^{-1} \boldsymbol{i}_s^s \tag{6}$$

The electromechanical torque, τ, produced by the machine is expressed

$$\tau = \frac{3}{2} p (L_d - L_q) i_d i_q, \tag{7}$$

where p is the number of pole pairs and L is the linearised inductance $L = \frac{\psi}{i}$.

B. Parameters

The parameters of the RSM used in the evaluation of the presented hybrid control scheme are listed in Table I. The rated speed is lowered from 1500 r/min to 1300 r/min, because of a limited DC link voltage (resulting from a limited 3-ϕ supply) which causes the SVPWM scheme to saturate not apply the reference voltage vector. This causes the AF estimator to fail, because it is dependent on the reference voltage vector in its determination of the electrical rotor angle.

When the machine is rotating above an appropriate speed and the load current is above 2 A_{peak} ($i_d = 1$ A @ rated current angle), the estimation is done using the AF method. Fig. 1 shows that this allows for at least 50% of the flux linkage at rated current to be present, which was found to be sufficient for estimation. Note that the method presented in [15] implemented constant field current control (using rated d-current up to base speed), which is less efficient.

The linearised and tangential ($\tilde{L}_s^r$) machine inductances in the rotor reference frame are shown in Fig. 2, as determined by FEM analysis. From this figure it is evident that at zero current the saliency ratio $(\tilde{L}_d - \tilde{L}_q)/2$ is small, which does not allow for position tracking using a saliency-based signal injection method such as AI. Therefore a reference saturation current of at least $i_q = 1.5$ A is used in this case, above which constant current angle control is implemented to ensure close to maximum efficiency (MTPA) [19].

From Fig. 2 it can be seen that the q-axis inductance, L_q, of the evaluated RSM is notably variable with change in current and cannot be used as a constant as is done in [15], even though the AF estimator is only in control when $i_q \geq 1.73$ A. Subsequently inductances L_d/L_q are determined every switching cycle by means of a lookup-table. This compensates for cross-magnetisation effects as well.

The financial assistance of the National Research Foundation (NRF) towards this research is hereby acknowledged. Opinions expressed and conclusions arrived at, are those of the author and are not necessarily to be attributed to the NRF.

TABLE I
RATED RSM DRIVE PARAMETERS.

Parameter	Value
Nominal Power	1.1 kW
Phase Current	3.54 A (RMS)
Rated mechanical speed (n_m)	1500 r/min*
Stator Phase Resistance (R_s)	5 Ω
Pole Pairs (p)	2
Current Angle (γ)	60°

* Reduced to 1300 r/min due to low DC link voltage.

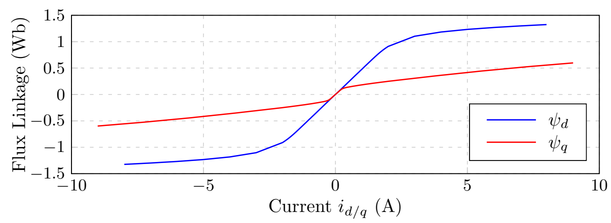

Fig. 1. Flux Linkage versus d/q-current.

III. THE ACTIVE FLUX BASED ESTIMATOR

The AF fundamental model estimation scheme used is relatively simple and has approximately the same estimation structure for all AC machines. It turns the RSM into a fictitious nonsalient-pole (isotropic) machine with the torque given as [15]

$$\tau = \frac{3}{2} p \psi_d^a i_q, \tag{8}$$

where $\psi_d^a = (L_d - L_q) i_d$ (see (7)) is the active flux. The active flux observer in the stator reference frame is defined as [7]

$$\hat{\boldsymbol{\psi}}_d^{as} = \int (\boldsymbol{v}_s^s - R_s \boldsymbol{i}_s^s + \boldsymbol{v}_{comp}).dt - L_q \boldsymbol{i}_s^s \tag{9}$$

$$= \psi_d^a \cos\theta_{\psi_d^a} + j\psi_d^a \sin\theta_{\psi_d^a}. \tag{10}$$

Equation (9) can be graphically understood by the steady state vector diagram shown in Fig. 3. Integrator drift is caused

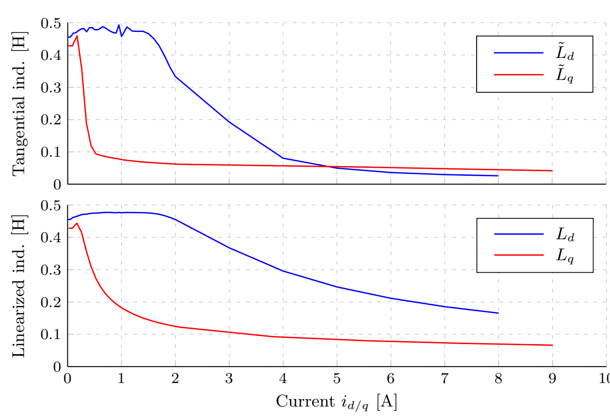

Fig. 2. Tangential/Linearised inductance versus d/q-current.

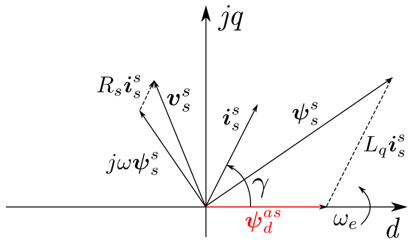

Fig. 3. The steady state active flux vector diagram.

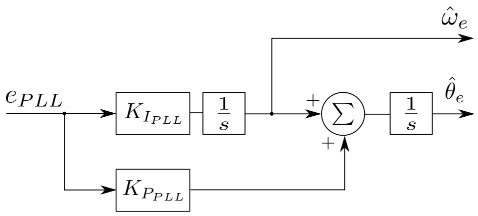

Fig. 4. PLL observer scheme with error signal input and estimation output.

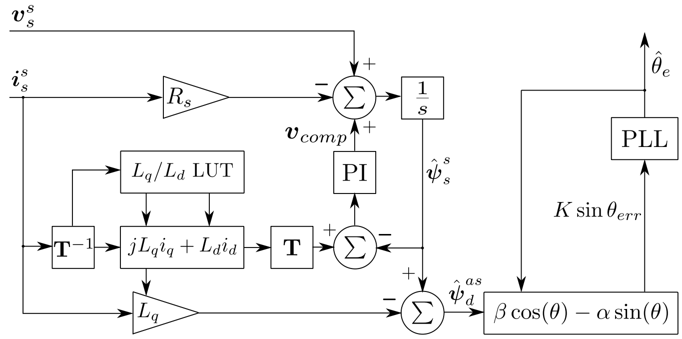

Fig. 5. Active Flux based estimation scheme block diagram.

by parameter estimation- and measurement errors [20]. This drift is rectified with a compensation voltage, $\boldsymbol{v}_{comp}$, which is a function of the voltage-flux and current-flux models of the machine defined as [15]

$$\boldsymbol{\psi}_s^{sv} = \int(\boldsymbol{v}_s^s - R_s\boldsymbol{i}_s^s + \boldsymbol{v}_{comp}).dt \tag{11}$$

and

$$\boldsymbol{\psi}_s^{si} = \mathbf{T}(L_di_d + jL_qi_q). \tag{12}$$

By feeding the difference of the two models through a PI compensator as in (13) $\hat{\boldsymbol{\psi}}_s^s = \boldsymbol{\psi}_s^{sv}$ which is predominantly equal to the current-flux model at low frequencies and the voltage-flux model at higher frequencies. This compensates for pure integrator offset and drift errors as well as stator resistance measurement errors [15]. Consequently, the estimated active flux vector can be calculated as in (14).

$$\boldsymbol{v}_{comp} = (K_P + \frac{K_I}{s})(\boldsymbol{\psi}_s^{si} - \boldsymbol{\psi}_s^{sv}) \tag{13}$$

$$\hat{\boldsymbol{\psi}}_d^{as} = \hat{\boldsymbol{\psi}}_s^s - L_q\boldsymbol{i}_s^s \tag{14}$$

The phase-locked loop (PLL) based observer scheme shown in Fig. 4 is used for the estimator derived herein, which results in the estimated electrical angle by feeding the error signal $K\sin\theta_{err}$ in (16) through a PI controller, forcing it to zero [21]. The complete AF based estimator is shown in Fig. 5 in block diagram format.

$$K\sin\theta_{err} = \psi_{d\beta}^a\cos\hat{\theta}_e - \psi_{d\alpha}^a\sin\hat{\theta}_e \tag{15}$$

$$= |\hat{\boldsymbol{\psi}}_d^{as}|\sin(\theta_{\hat{\psi}_d^{as}} - \hat{\theta}_e) \tag{16}$$

IV. The Arbitrary Injection Based Estimator

The AI saliency-based method used is a rather novel concept relying on the presence of a current derivative with the advantage of requiring no predetermined injection signal shape, allowing the use of a smaller fraction of the DC bus voltage [11]. This scheme enables elimination of some machine parameters in the position estimation algorithm as well as on-line parameter identification, allowing position estimation without any knowledge of machine parameters [22].

The flux linkage derivative is calculated with (1) and (6) as

$$\frac{d\boldsymbol{\psi}_s^s}{dt} = \boldsymbol{L}_s^s\frac{d\boldsymbol{i}_s^s}{dt} + \frac{d\boldsymbol{L}_s^s}{dt}\boldsymbol{i}_s^s \tag{17}$$

with $\boldsymbol{L}_s^s = \mathbf{T}\boldsymbol{L}_s^r\mathbf{T}^{-1}$

$$\boldsymbol{L}_s^s = L_\Sigma\mathbf{I} + L_\Delta\mathbf{S}(\theta_e) \tag{18}$$

where

$$L_\Sigma = \frac{\tilde{L}_d + \tilde{L}_q}{2}; L_\Delta = \frac{\tilde{L}_d - \tilde{L}_q}{2}$$
$$\mathbf{S}(\theta_e) = \begin{bmatrix}\cos 2\theta_e & \sin 2\theta_e\\ \sin 2\theta_e & -\cos 2\theta_e\end{bmatrix}$$
$$\frac{d\boldsymbol{L}_s^s}{dt} = \frac{\partial\boldsymbol{L}_s^s}{\partial\theta_e}\omega_e.$$

Solving for the current/time derivative

$$\frac{d\boldsymbol{i}_s^s}{dt} = \boldsymbol{L}_s^{s-1}\left(\boldsymbol{v}_s^s - R_s\boldsymbol{i}_s^s - \omega_e\frac{\partial\boldsymbol{L}_s^s}{\partial\theta_e}\boldsymbol{i}_s^s\right) \tag{19}$$

where the inverse of the inductance in the stator reference frame equals

$$\boldsymbol{L}_s^{s-1} = Y_\Sigma\mathbf{I} + Y_\Delta\mathbf{S}(\theta_e) \tag{20}$$

with admittance

$$Y_\Sigma = \frac{Y_d + Y_q}{2}; Y_\Delta = \frac{Y_d - Y_q}{2}, Y = \frac{1}{\tilde{L}}.$$

The current progression of an isotropic machine $\Delta\hat{\boldsymbol{i}}_{s\Sigma}^s$ (with salient admittance consciously neglected ($Y_\Delta = 0$)) can be predicted by taking $\frac{d\boldsymbol{i}_s^s}{dt} = \frac{\Delta\boldsymbol{i}_s^s}{\Delta t}$, resulting from (19) to [11]

$$\Delta\hat{\boldsymbol{i}}_{s\Sigma}^s[n] = Y_\Sigma\left(\boldsymbol{v}_s^s[n_1] - R_s\boldsymbol{i}_s^s[n_1] - \left(\omega_e\frac{\partial\boldsymbol{L}_s^s}{\partial\theta_e}\boldsymbol{i}_s^s\right)[n_1]\right)\Delta t. \tag{21}$$

$[n_1] = [n-1]$ refers to the previous calculation interval. In contrast, the measured current progression of the salient pole machine is calculated using (22).

$$\Delta\boldsymbol{i}_s^s[n] = \boldsymbol{i}_s^s[n] - \boldsymbol{i}_s^s[n_1] \tag{22}$$

A. Parameter Reduction And Position Estimation

From [11], assuming that the resistive voltage $R_s \boldsymbol{i}_s^s$ and the EMF vector $\omega_e \frac{\partial \boldsymbol{L}_s^s}{\partial \theta_e} \boldsymbol{i}_s^s$ in (21) stay constant within two switching cycles ($2\Delta t = 2t_s$), the difference between consecutive predicted current progressions can be calculated using the stator voltage as

$$\Delta \hat{\boldsymbol{i}}_{s\Sigma}^s[n_1] - \Delta \hat{\boldsymbol{i}}_{s\Sigma}^s[n_2] = Y_\Sigma(\boldsymbol{v}_s^s[n_1] - \boldsymbol{v}_s^s[n_2])\Delta t$$

$$\Delta(\Delta \hat{\boldsymbol{i}}_{s\Sigma}^s) = Y_\Sigma(\Delta \boldsymbol{v}_s^s)\Delta t. \tag{23}$$

$$\Delta(\Delta \boldsymbol{i}_s^s) = \boldsymbol{i}_s^s[n] - 2\boldsymbol{i}_s^s[n_1] + \boldsymbol{i}_s^s[n_2] \tag{24}$$

The difference $\Delta(\Delta \boldsymbol{i}_s^s)$ refers to the measured stator current progressions.

The high-frequency component, $\Delta \boldsymbol{i}_{HF}^s$, in (26) of the difference between the measured and predicted current progressions, $\boldsymbol{i}_{\Delta err}^s$, in (25) is an angle dependent term and can be predicted using the estimated angle of a PLL according to [18] and simplified as

$$\boldsymbol{i}_{\Delta err}^s = \Delta(\Delta \boldsymbol{i}_s^s) - \Delta(\Delta \hat{\boldsymbol{i}}_{s\Sigma}^s), \tag{25}$$

$$\Delta \boldsymbol{i}_{HF}^s = HPF(\boldsymbol{i}_{\Delta err}^s), \tag{26}$$

$$\Delta \hat{\boldsymbol{i}}_{HF}^s = Y_\Delta \mathbf{S}(\theta_{PLL})(\boldsymbol{v}_s^s - R_s \boldsymbol{i}_s^s)\Delta t \tag{27}$$

$$\Delta \hat{\boldsymbol{i}}_{HF}^s = Y_\Delta \mathbf{S}(\theta_{PLL})\Delta \boldsymbol{v}_s^s \Delta t. \tag{28}$$

Consequently, assuming the PLL angle is correct, the vectors $\Delta \boldsymbol{i}_{HF}^s$ and $\Delta \hat{\boldsymbol{i}}_{HF}^s$ will be oriented the same way. The PLL is closed by taking the error as the vector product of these vectors as

$$e_{PLL} = \Delta \boldsymbol{i}_{HF}^{s\ T} \mathbf{J}\, \Delta \hat{\boldsymbol{i}}_{HF}^s, \ \mathbf{J} = \mathbf{T}(\frac{\pi}{2}),$$

which will be equal to zero when $\theta_{PLL} = \theta_e$. Then, considering orientation only

$$e_{PLL} = \Delta \boldsymbol{i}_{HF}^{s\ T} \mathbf{J}\ \mathbf{S}(\theta_{PLL})\Delta \boldsymbol{v}_s^s. \tag{29}$$

This error is fed into a PLL observer scheme with the same structure as shown in Fig. 4 to result in the estimated angle and angular frequency.

B. Injection Sequence and Parameter Identification

Since this estimation scheme requires the presence of a current time derivative in the stator reference frame, a square wave spatially rotating 120° in the stator reference frame every switching cycle (t_s) is injected. This allows online admittance calculation because it is stepped in integer fractions of 360° and the high frequency yields more frequent position information, larger separation from the current controller bandwidth and lower audible noise [11].

The injected voltage vector superimposed on the stator voltage vector is shown in Fig. 6 with the outline of the hexagon being the maximum voltage that can be applied using space vector pulse width modulation.

From (23), (24) and (29) the only remaining machine parameter for position estimation is the mean admittance Y_Σ. The resulting current slope for an applied voltage vector represents the admittance for that voltage excitation. From [22]

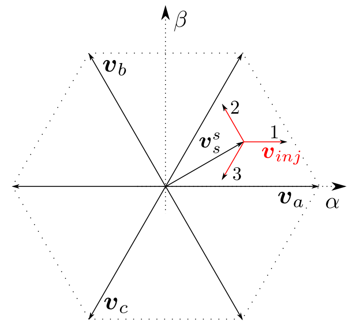

Fig. 6. Injected voltage vector diagram inside the limits of Space Vector PWM.

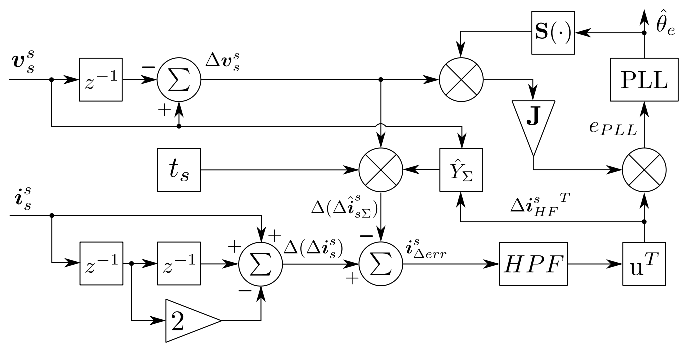

Fig. 7. Arbitrary Injection based estimation scheme block diagram.

the admittance for a certain switching cycle can be calculated as

$$\hat{Y}_{tX} = \frac{\Delta \boldsymbol{i}_{HF}^{s\ T} \boldsymbol{v}_s^s}{\boldsymbol{v}_s^{s\,T} \boldsymbol{v}_s^s}, X = 1, 2, 3. \tag{30}$$

Since the injected voltages are symmetrically distributed the mean admittance estimation equals

$$\hat{Y}_\Sigma = \frac{\hat{Y}_{t1} + \hat{Y}_{t2} + \hat{Y}_{t3}}{3}. \tag{31}$$

The complete AI based estimator is shown in Fig. 7 in block diagram format.

V. The Hybrid Controller

The new hybrid estimation scheme derived herein combines the AF and AI methods using a hysteresis approach shown in Fig. 8. The regions were chosen using the following criteria:

- At least 500 r/min mechanical rotor speed to enter AF (this allows fast enough PLL synchronisation)
- At least 200 r/min to maintain AF estimation
- At least 1 A d-axis saturation current ($i_s = 2$ A at $\gamma = 60°$) for AF
- A 500 mA current buffer for hysteresis

Switching between estimation schemes only occurs when crossing the edges of the hysteresis region in the direction of the arrows shown. This eliminates back and forth switching between states at a certain operating point.

The two shaft-connected machines used in the testing and evaluation of the proposed method are shown in Fig. 9. The

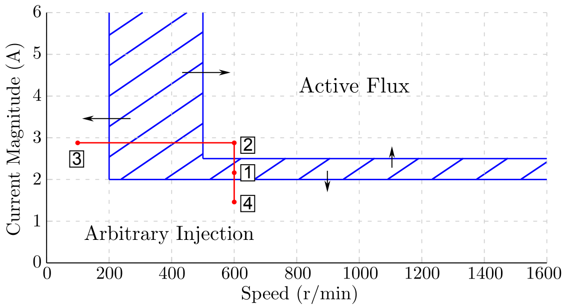

Fig. 8. Hybrid estimation scheme regions with highlighted hysteresis region and operating points for the practical tests shown in Fig. 11.

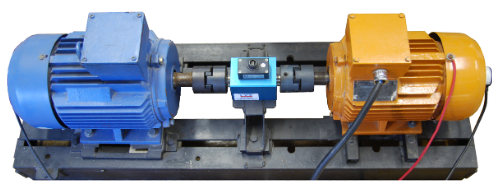

Fig. 9. The machines used for practical tests. RSM - Orange, IM - Blue.

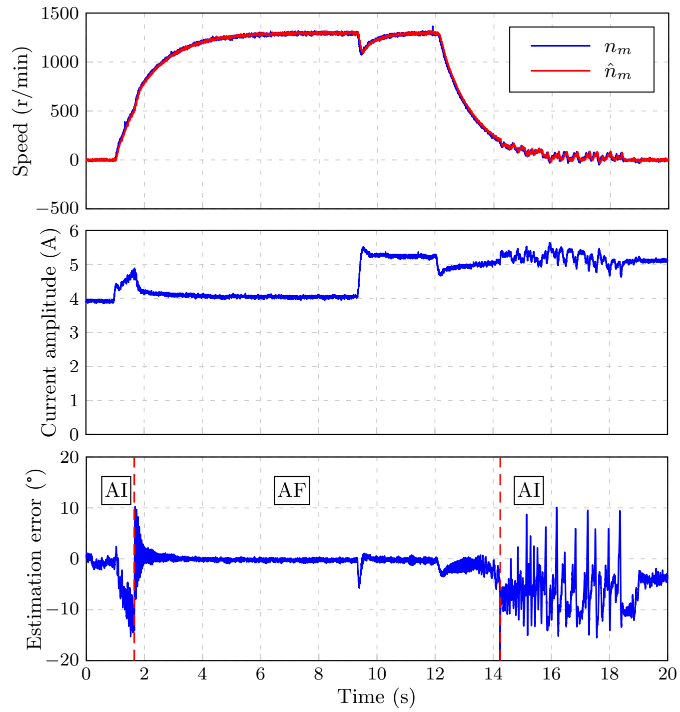

Fig. 10. Sensorless speed control at about 80% load from standstill to rated speed followed by load step to about 105% load showing mechanical speed, reference current, and estimated angle error versus time.

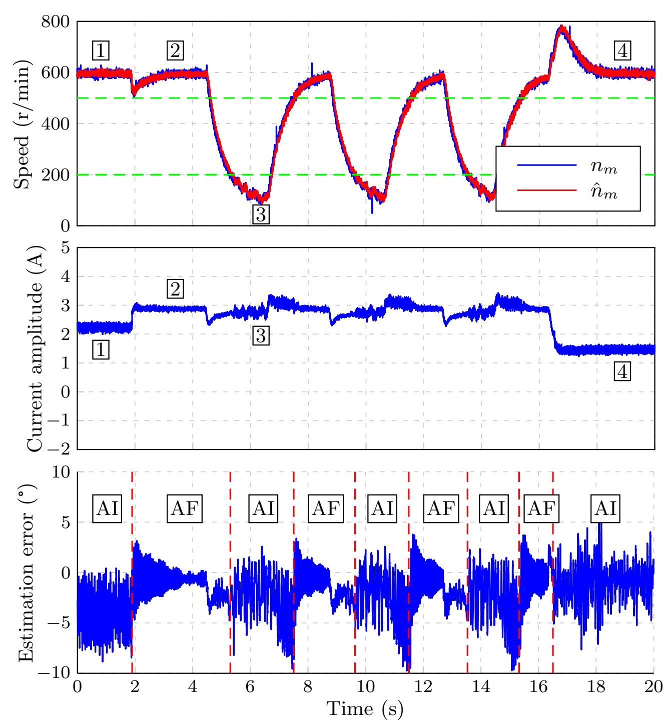

Fig. 11. Sensorless speed control with about 60% load from standstill to rated speed showing mechanical rotor speed, current amplitude, and estimated angle error versus time.

RSM is connected via a torque sensor to an induction machine (IM). Two DC link connected inverters are used to drive both machines. The switching signals for the inverters are applied by two Linux-based rapid prototyping systems on which the complete control algorithm runs.

Field-oriented control is implemented on the RSM with constant current angle, $\gamma = \gamma_{rated}$, maintained (except at low currents for q-axis saturation) for close to maximum efficiency.

VI. Measured Results

Fig. 10 shows a 80% load sensorless standstill to rated speed control step of the RSM followed by an increased load step (by the IM) to about 105%. The hybrid controller starts with AI at standstill and switches to AF and back to AI at 500 r/min and 200 r/min respectively. This test showcases sensorless speed control in the entire rated speed and current range of the RSM.

Sensorless speed control of the RSM around the hysteresis region is shown in Fig. 11 with about 60% load applied. It can be seen that the control switches reliably between estimation schemes and that speed control is stable at the application initially and removal of the load at the end. Fig. 8 shows the operating points of this test around the hysteresis region.

Fig. 12 shows a 20% to 100% load control step at $t = 45$ ms at rated speed. The estimated angles shown are uncompensated for load in order to show the effects thereof. This figure shows that the sensorless current control is stable with instant switch-over between estimation schemes and settles within 5 ms.

VII. Conclusions

In this paper a hybrid AF plus AI position estimation scheme is proposed and practically implemented for position sensorless control of the RSM drive. From the research and results the following conclusions are drawn:

- With the proposed hybrid scheme, position sensorless control of the RSM is demonstrated from standstill to

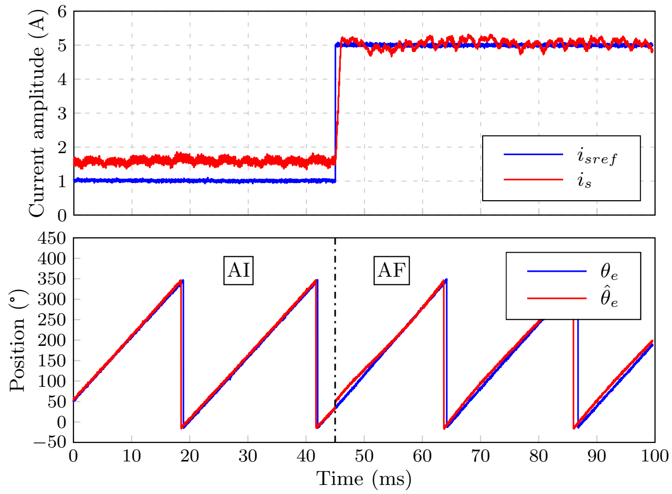

Fig. 12. 20% to 100% sensorless load control step at rated speed showing current response and uncompensated estimated angles versus time.

rated speed in the entire rated load range. For the investigated 1.1 kW drive system the load control is stable and settles in about 10 ms for a large speed step input crossing the changeover region.

- It is found that with maximum TPA control the AF position estimation scheme cannot be used at zero or low loads, even if the machine has a good saliency because a minimum amount of d-axis current is required. This distinguishes the AF method drastically from the fundamental scheme method of [6] where a minimum amount of q-axis current is required (which becomes very small if the saliency of the machine is good).
- With maximum TPA control it is found that the updating AF scheme proposed by [15] cannot be used for a normal transverse laminated rotor RSM because the HFI method requires q-axis saturation current.
- It is found that the AI method can be used at rated speeds, but only at low loads because the AI estimator has a growing estimation error at higher speeds under load caused by saliency shift.
- The hybrid controller can be made more dynamic by implementing a mechanical model-based PLL for the AF method to reduce estimation errors during speed transients.

References

[1] I. Boldea, *Reluctance Synchronous Machines and Drives*, ser. Monographs in electrical and electronic engineering. Clarendon Press, 1996.

[2] M. Prins, C. Vorster, and M. Kamper, "Reluctance synchronous and field intensified-pm motors for variable-gear electric vehicle drives," in *Energy Conversion Congress and Exposition (ECCE), 2013 IEEE*, 2013, pp. 657–664.

[3] S. Tokunaga and K. Kesamaru, "Fem simulation of novel small wind turbine generation system with synchronous reluctance generator," in *Electrical Machines and Systems (ICEMS), 2011 International Conference on*, 2011, pp. 1–6.

[4] A. Vagati, "The synchronous reluctance solution: a new alternative in ac drives," in *Industrial Electronics, Control and Instrumentation, 1994. IECON '94., 20th International Conference on*, vol. 1, 1994, pp. 1–13 vol.1.

[5] T. Matsuo and T. Lipo, "Field oriented control of synchronous reluctance machine," in *Power Electronics Specialists Conference, 1993. PESC '93 Record., 24th Annual IEEE*, 1993, pp. 425–431.

[6] P. Landsmann, R. Kennel, H. de Kock, and M. Kamper, "Fundamental saliency based encoderless control for reluctance synchronous machines," in *Electrical Machines (ICEM), 2010 XIX International Conference on*, 2010, pp. 1–7.

[7] I. Boldea and S. Agarlita, "The active flux concept for motion-sensorless unified ac drives: A review," in *Electrical Machines and Power Electronics and 2011 Electromotion Joint Conference (ACEMP), 2011 International Aegean Conference on*, 2011, pp. 1–16.

[8] A. Ejlali, S. Taravat, and J. Soleimani, "Comparative study on control strategy of dtfc based on active flux concept and dtc for ipmsm applied to traction motor," in *Power Electronics, Electrical Drives, Automation and Motion (SPEEDAM), 2012 International Symposium on*, 2012, pp. 200–206.

[9] A. Ravikumar Setty, S. Wekhande, and K. Chatterjee, "Comparison of high frequency signal injection techniques for rotor position estimation at low speed to standstill of pmsm," in *Power Electronics (IICPE), 2012 IEEE 5th India International Conference on*, 2012, pp. 1–6.

[10] D. Raca, P. Garcia, D. Reigosa, F. Briz, and R. Lorenz, "A comparative analysis of pulsating vs. rotating vector carrier signal injection-based sensorless control," in *Applied Power Electronics Conference and Exposition, 2008. APEC 2008. Twenty-Third Annual IEEE*, 2008, pp. 879–885.

[11] D. Paulus, P. Landsmann, and R. Kennel, "Sensorless field- oriented control for permanent magnet synchronous machines with an arbitrary injection scheme and direct angle calculation," in *Sensorless Control for Electrical Drives (SLED), 2011 Symposium on*, 2011, pp. 41–46.

[12] G. Andreescu and C. Schlezinger, "Enhancement sensorless control system for pmsm drives using square-wave signal injection," in *Power Electronics Electrical Drives Automation and Motion (SPEEDAM), 2010 International Symposium on*, 2010, pp. 1508–1511.

[13] W. Villet, M. Kamper, P. Landsmann, and R. Kennel, "Evaluation of a simplified high frequency injection position sensorless control method for reluctance synchronous machine drives," in *Power Electronics, Machines and Drives (PEMD 2012), 6th IET International Conference on*, 2012, pp. 1–6.

[14] C. Silva, G. Asher, and M. Sumner, "Hybrid rotor position observer for wide speed-range sensorless pm motor drives including zero speed," *Industrial Electronics, IEEE Transactions on*, vol. 53, no. 2, pp. 373–378, 2006.

[15] S.-C. Agarlita, I. Boldea, and F. Blaabjerg, "High-frequency-injection-assisted "active-flux"-based sensorless vector control of reluctance synchronous motors, with experiments from zero speed," *Industry Applications, IEEE Transactions on*, vol. 48, no. 6, pp. 1931–1939, 2012.

[16] E. Capecchi, P. Guglielmi, M. Pastorelli, and A. Vagati, "Position-sensorless control of the transverse-laminated synchronous reluctance motor," *Industry Applications, IEEE Transactions on*, vol. 37, no. 6, pp. 1768–1776, 2001.

[17] W. Villet, M. Kamper, P. Landsmann, and R. Kennel, "Hybrid position sensorless vector control of a reluctance synchronous machine through the entire speed range," in *Power Electronics and Motion Control Conference (EPE/PEMC), 2012 15th International*, 2012, pp. LS4b–1.1–1–LS4b–1.1–7.

[18] P. Landsmann, D. Paulus, P. Stolze, and R. Kennel, "Saliency based encoderless predictive torque control without signal injection for a reluctance synchronous machine," in *Power Electronics and Motion Control Conference (EPE/PEMC), 2010 14th International*, 2010, pp. S1–10–S1–17.

[19] R. Betz, R. Lagerquist, M. Jovanovic, T. J. E. Miller, and R. Middleton, "Control of synchronous reluctance machines," *Industry Applications, IEEE Transactions on*, vol. 29, no. 6, pp. 1110–1122, 1993.

[20] J. Holtz and J. Quan, "Sensorless vector control of induction motors at very low speed using a nonlinear inverter model and parameter identification," *Industry Applications, IEEE Transactions on*, vol. 38, no. 4, pp. 1087–1095, 2002.

[21] L. Harnefors and H.-P. Nee, "A general algorithm for speed and position estimation of ac motors," *Industrial Electronics, IEEE Transactions on*, vol. 47, no. 1, pp. 77–83, 2000.

[22] P. Landsmann, C. Hackl, and R. Kennel, "Eliminating all machine parameters in encoderless predictive torque control without signal injection," in *Electric Machines Drives Conference (IEMDC), 2011 IEEE International*, 2011, pp. 1259–1264.